



Inverse design and demonstration of an ultracompact broadband dual-mode 3 dB power splitter

WEIJIE CHANG,¹ XINSHU REN,¹ YINGQUAN AO,¹ LONGHUI LU,¹ MENGFAN CHENG,¹ LEI DENG,¹ DEMING LIU,¹ AND MINMING ZHANG^{1,2*}

¹School of Optical and Electrical Information, Huazhong University of Science and Technology, Wuhan 430074, China

²Wuhan National Laboratory for Optoelectronics, Huazhong University of Science and Technology, Wuhan 430074, China

*mmz@hust.edu.cn

Abstract: An ultracompact broadband dual-mode 3 dB power splitter using inverse design method for highly integrated on-chip mode (de) multiplexing system is proposed and experimentally demonstrated. A dual-mode convertor based on subwavelength axisymmetric three-branch waveguide is utilized to convert TE₀ and TE₁ to three intermediate fundamental modes. The axisymmetric topology constraint of the nanostructures enables the optimized device to achieve a strict 50:50 splitting ratio over a broad wavelength range from 1.52 to 1.60 μm. The fabricated device occupied a compact footprint of only 2.88 μm × 2.88 μm. The measured average excess losses and crosstalks for both modes were respectively less than 1.5 dB and -20 dB from 1.52 to 1.58 μm for both TE₀ and TE₁, which are consistent with the numerical simulations.

© 2018 Optical Society of America under the terms of the [OSA Open Access Publishing Agreement](#)

1. Introduction

Mode-division multiplexing (MDM) on silicon-on-insulator (SOI) platform, as a more promising and attractive technology, has attracted substantial attention to further increase the transmission capacity of on-chip optical interconnect [1]. To realize on-chip MDM systems, various key building blocks have been reported, such as mode (de) multiplexers ((DE) MUX) [2–6], mode switch [7, 8], multimode waveguide crossing [9, 10] and multimode bent waveguides [11–13]. However, a dual-mode power splitter with compact footprint and broad bandwidth, as an essential component for realizing the densely integrated MDM optical interconnect network, has been rarely addressed due to the complex mode coupling for high order modes. Recently, an integrated dual-mode 3 dB power coupler based on tapered directional coupler was present [14], which could work at the wavelength of 1.55 μm for both TM₀ and TM₁. However, it is bandwidth-limited even though the tapered directional coupler is adopted. To achieve the broadband property, multimode power splitters based on symmetric Y-junctions were proposed [15, 16]. In [15], an input N^{th} -order mode has to be converted to a $2N^{\text{th}}$ -order mode using cascaded mode convertors before power division by a symmetric Y-junction. In [16], an adiabatic coupler was used in the input stage to convert the input mode to an intermediate high order supermode and realize 3 dB power splitter by an S-bend based Y-junction. However, adiabatic components employed in both types of devices lead to a large device footprint, which may prevent further potential application in dense and large-scale on-chip photonic integration.

Recently, free-form metamaterials based on inverse design potentially offer an effective approach to design ultracompact and highly functional devices simultaneously [17–21]. In contrast to the traditional device design, the inverse design approach can flexibly engineer the refractive index distribution and manipulate light field at a deep subwavelength scale to realize a variety of ultracompact integrated devices. However, due to the lag effect of plasma etching process, etching patterns with small and random feature sizes of the inverse designed

nanostructures may probably introduce large fabrication errors. To implement nanostructured devices robust to fabrication tolerances, one may use the photonic-crystal-like (PhC-like) subwavelength structure [22] or fabrication-constrained topology optimization method [23] for nanophotonic inverse design.

In this work, we propose a broadband dual-mode 3 dB power splitter based on axisymmetric three-branch waveguides, and realize its ultracompact version based on the PhC-like subwavelength structure using an inverse design approach. The basic idea of the proposed device is that we first convert the two input normal modes to six intermediate fundamental modes (IFMs), and finally synthesize the two output normal modes in each output waveguide from the phase-shifted IFMs, respectively. To further decrease the footprint, we employ PhC-like subwavelength structure to design the device by inverse design method. We find that, in the inverse design of dual-mode 3 dB power splitter using axisymmetric topology constraint, the optimization iteration based on random initial patterns usually converges to optimized subwavelength structures which are equivalent to the proposed waveguide device model. In addition, the axisymmetric optical field distribution contributes to a strict 50: 50 splitting ratio for both modes. The footprint of the fabricated device is $2.88 \times 2.88 \mu\text{m}^2$, which may be the most compact dual-mode 3 dB power splitter that has been reported to the best of our knowledge. The measured excess losses (ELs) and crosstalks (XTs) for both modes are less than 1.5 dB and -20 dB from 1540 to 1580 nm, respectively.

2. Design, optimization, and simulations

2.1 Dual-mode 3 dB power splitter based on conventional waveguide

Figure 1(a) schematically shows the dual-mode 3 dB power splitter, based on conventional waveguides, which is composed of three axisymmetric three-branch waveguides, three symmetric Y-junctions and two π phase shifters.

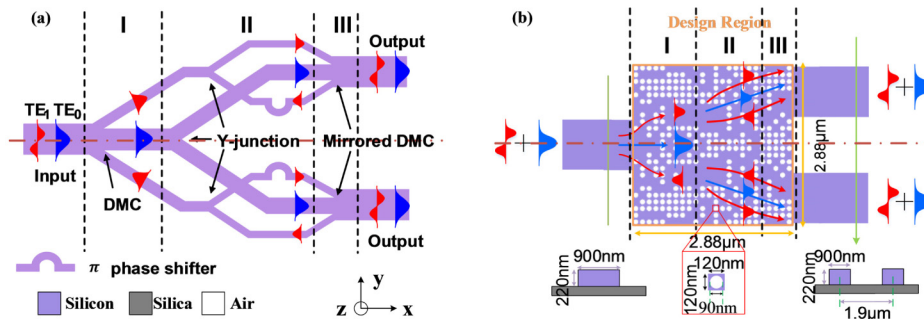


Fig. 1. (a) Dual-mode 3 dB power splitter assisted with DMCs based on conventional waveguides. (b) The proposed dual-mode power splitter assisted with DMCs, based on subwavelength structure.

The structure of the proposed device can be divided into three stages. In the stage I, the axisymmetric three-branch waveguide works as a dual-mode convertor (DMC), which converts the fundamental transverse electric mode (TE_0) to an intermediate fundamental mode in the middle branch (IFM_{1m}), and splits the first-order transverse electric mode (TE_1) into two anti-phase IFMs in the upper and lower branches (IFM_{1u} and IFM_{1l}), respectively. In the stage II, the IFM_{1u} is further split into two anti-phase IFMs via one symmetric Y-junction and one π phase shifter, then both anti-phase IFMs are respectively injected into the upper and lower branches of the upper mirrored DMC in the stage III to excite the TE_1 mode in the upper output waveguide. Meanwhile, the IFM_{1m} is split into two in-phase IFMs using a Y-junction in the stage II and the upper IFM is injected into the middle branch of the upper mirrored DMC in the stage III to excite the TE_0 mode in the upper output waveguide. The two

normal modes in the lower output waveguide are excited in the similar way. Notably, benefiting from the axisymmetric structure, a strict 50: 50 power splitting ratio for both modes can be achieved.

The DMC is a key component of the dual-mode 3 dB power splitter. As shown in Fig. 2(a), the layout of DMC is axisymmetric. Each DMC consists of a dual-mode stem and three single-mode branches with different widths. The waveguide widths of the two lateral branches and the middle one are W_0 and W_1 , respectively. The gap between adjacent branches increases from 0 to W_{gap} gradually, forming an adiabatic coupled waveguide system with a coupling length of L . Due to close modal effective refraction index match, TE_0 and TE_1 are first evolved into the corresponding even supermode $\text{T}_{\text{SM}0}$ and odd supermode $\text{T}_{\text{SM}1}$ in the adiabatic coupled waveguide system region, respectively. Then the $\text{T}_{\text{SM}0}$ and $\text{T}_{\text{SM}1}$ are converted to the IFM in the middle output waveguide and two anti-phase IFMs in the two lateral output waveguides. To avoid the modal coupling, the W_{gap} should be larger than 1 μm . The effective indices of $\text{T}_{\text{SM}0}$ and $\text{T}_{\text{SM}1}$ as a function of W_0 , W_1 and W_{gap} are presented in Figs. 2(b)-2(d), respectively. The effective indices of TE_0 and TE_1 in the stem waveguide are 2.6 and 2.28, respectively. Thus, to guarantee only supporting single mode in the multi-branches and satisfy close modal match, W_0 and W_1 are chosen to 550 nm and 450 nm, respectively. The high-efficiency mode conversion in a short adiabatic coupling length could be achieved in this way. We also simulate the adiabatic evolution in the DMC with different adiabatic coupling lengths. The calculated mode conversion efficiencies for the TE_0 and TE_1 launched into the stem waveguide as a function of the coupler length are shown in Fig. 2(f). Therefore, L should be more than 100 μm to achieve mode conversion with a high efficiency up to 98%. The other components of the dual-mode 3 dB splitter including broadband single-mode symmetric Y-junctions, broadband 2×2 waveguide crossings and broadband π phase shifters could be designed and optimized based on the conventional waveguide [24–26].

Theoretically, a broadband dual-mode 3 dB power splitter could be achieved with these waveguide components, as illustrated in Fig. 1(a). However, a long adiabatic evolution length ($> 100 \mu\text{m}$) is usually required for each DMC and the total length of the device based on the conventional waveguide model may be larger than 200 μm , which prevents its potential application in dense and large-scale on-chip photonic integration.

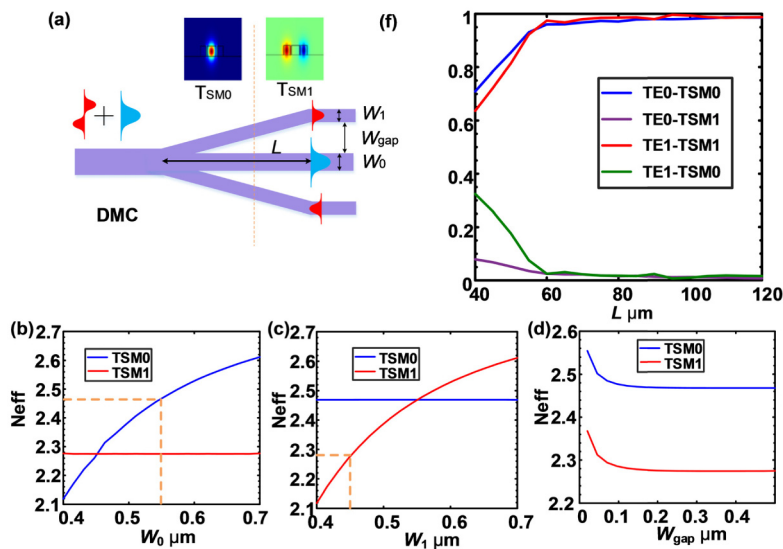


Fig. 2. (a) The schematic of DMC based on conventional waveguide. (b) For $W_{\text{gap}} = 200 \text{ nm}$, $W_1 = 450 \text{ nm}$, mode effective index with different W_0 (c) For $W_{\text{gap}} = 200 \text{ nm}$, $W_0 = 550 \text{ nm}$, mode effective index as a function of W_1 (d) For $W_0 = 550 \text{ nm}$, $W_1 = 450 \text{ nm}$, mode effective index with different W_{gap} (f) Transmission spectra as a function of L .

2.2 Dual-mode 3 dB power splitter based on subwavelength structure

In this work, the PhC-like subwavelength structure is used for inverse design of an ultracompact dual-mode 3 dB power splitter. For an ideal dual-mode 3 dB power splitter with an axisymmetric layout, the distributions of the electric field and the dielectric permittivity inside the device should also be axisymmetric. Therefore, the axisymmetric topology constraint is enforced during the inverse design process, which maintains an axisymmetric pattern in each round of iteration.

As shown in Fig. 1(b), the proposed 3 dB power splitter based on the PhC-like subwavelength structure is designed on a silicon-on-insulator platform with 220 nm-thick air-cladded top silicon layer. The widths of the input waveguide and output waveguides are 900 nm. The gap between the two output waveguides should be larger than 1 μm to avoid modal crosstalk. The inverse design region composed of 24×24 discrete pixels occupies a compact footprint of only $2.88 \times 2.88 \mu\text{m}^2$. Each pixel is a square of $120 \times 120 \text{ nm}^2$ with a circular hole. The hole has a radius of 45 nm and a depth of 220 nm. Each hole can be occupied by silicon or air. The nonlinear direct-binary-search (DBS) optimization algorithm is utilized to decide the material of each hole to be silicon or air one by one and the figure-of-merit (FOM) is introduced to evaluate the optimized performance [18]. We randomly chose one pixel to change its occupied material (silicon or air), and calculate the FOM. If the FOM increases, then the changed material will be reserved. Otherwise, the pixel goes back to the original material. A 3D finite-difference time-domain (FDTD) method via a commercial software (Lumerical FDTD Solutions) is used to calculate the FOM [27]. The FOM in our simulation is defined as:

$$\text{FOM} = 1 - (1 - \alpha) \cdot \frac{1}{2M} \cdot \sum(|t_1 - 0.5| + |t_2 - 0.5|) - \alpha \cdot \frac{1}{2M} \sum(x_1 + x_2), \quad (1)$$

where t_1 and t_2 are the transmittances of TE_0 and TE_1 , respectively. Likewise, x_1 and x_2 are the conversion efficiencies of input TE_0 -output TE_1 and input TE_1 -output TE_0 , respectively. M denotes the number of wavelength and three wavelengths over an operating bandwidth of 80 nm are taken into consideration in simulations. Actually, the second and third terms in the right of Eq. (1) are used to optimize average excess losses and crosstalks for both modes, respectively. α , a weighted coefficient over a range from 0 to 1, is utilized to achieve a tradeoff between excess losses and crosstalks. For an ideal dual-mode 3 dB power splitter, the FOM is 1.

Considering the axisymmetric topology constraint, only the upper half of the pattern need to be optimized in each round of optimization based on the DBS algorithm. When the FOM exhibits no great improvement (< 1% for our case), the optimization process terminates. We first set $\alpha = 0$ to optimize the EL performance separately. Using the optimized pattern under $\alpha = 0$ as the new initial pattern, we set $\alpha = 0.25$ and then re-optimize the device based on the same algorithm to get the final optimized pattern which could reach a compromise between ELs and XTs. The inverse design takes about 28 hours on a computer with an 8-core central processing unit (Intel Xeon E5-2637).

As illustrated in Figs. 3(a) and 3(b), the working mechanism of the inverse-designed subwavelength device is equivalent to that of the conventional waveguide-based 3 dB power splitter in Fig. 1(a), while the footprint of the subwavelength scheme is reduced by about two orders of magnitude. The optical field evolution of both TE_0 and TE_1 in the optimized nanostructures can be also divided into three stages. In the stage I, the nanostructured DMC converts TE_0 to an IFM and splits TE_1 into two anti-phase IFMs, respectively. In the stage II, the IFM is further split into two in-phase IFMs by a nanostructured Y-junction while the anti-phase IFMs are further split into two pair of anti-phase IFMs via two axisymmetric nanostructured Y-junctions and two π phase shifters. In the stage III, these six IFMs finally synthesize the two output normal modes in each output waveguide via the mirrored

nanostructured DMC. Moreover, the axisymmetric topology constraint of the nanostructures could ensure the optical field distribution to be absolutely axisymmetric. A strict 50: 50 power splitter for both TE_0 and TE_1 can be obtained. Thus, an ultracompact broadband 3 dB splitter for both modes is achieved in this way. The simulated performance is shown in Figs. 3(c) and 3(d). The ELs of both TE_0 and TE_1 are less than 0.9 dB. The XTs for TE_0 and TE_1 at output port are lower than -20 dB and -24 dB over the wavelength range from 1520 to 1580 nm, respectively.

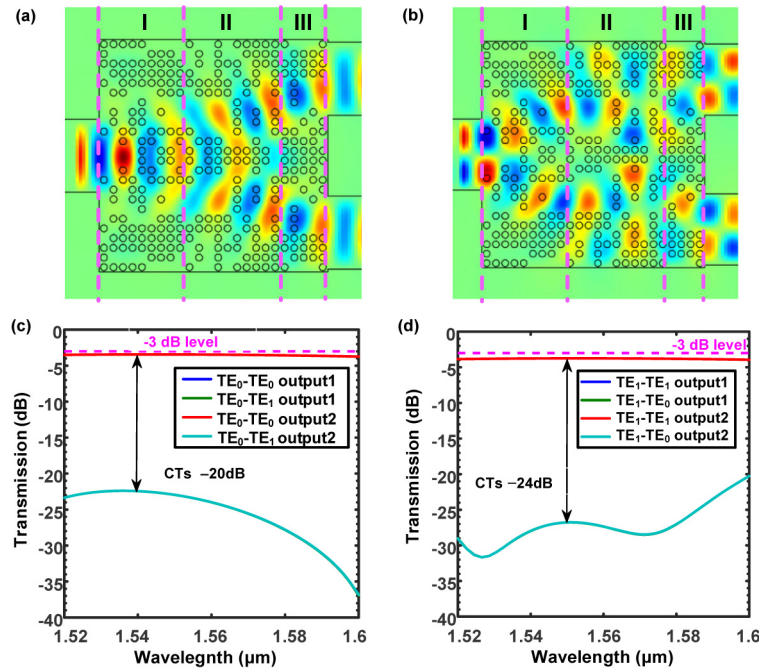


Fig. 3. (a) and (b) Simulated optical field evolutions of H_z for TE_0 and TE_1 , respectively. (c) and (d) Simulated transmission spectra for the MUX and the MDM system, respectively.

Generally, optimization algorithms for inverse design are sensitive to the initial pattern, and the optimized patterns usually seem like irregular and random [17, 18]. Here, under the axisymmetric topology constraint, we simulate and characterize several inverse-designed optimization patterns with random-generated and different initial patterns. The random initial patterns are generated by MATLAB. First, we use the *rand* function to obtain a matrix with uniformly randomly distributed values from 0 to 1. Then we convert it to a binary matrix: if the matrix element value is less than 0.5, it will be set to 0 (The corresponding occupied material is air). Otherwise, it will be set to 1 (The corresponding occupied material is silicon). The initial patterns and corresponding optimized patterns are shown in Figs. 4(a)-4(b), Figs. 4(e)-4(f) and Figs. 4(i)-4(j), respectively. The out-of-plane magnetic fields (H_z) at 1560 nm calculated for both TE_0 and TE_1 transmitted through the device are illustrated in Figs. 4(c)-4(d), Figs. 4(g)-4(h) and Figs. 4(k)-4(l), respectively. The FOMs for all the patterns after every iteration are given in Fig. 4(m). The corresponding transmission spectra for TE_0 and TE_1 of the three optimized devices are shown in Figs. 4(n) and 4(o), respectively. We select the pattern with best performance as the final pattern of the subwavelength dual-mode 3 dB power splitter. For all inverse-designed devices based on different random initial patterns, we can find that the optimization patterns vary widely and their performance are also different. But it is very interesting that the optical field evolution of the two modes in all optimized patterns is almost identical and equivalent to the mode evolution of the conventional waveguide model in Fig. 1(a).

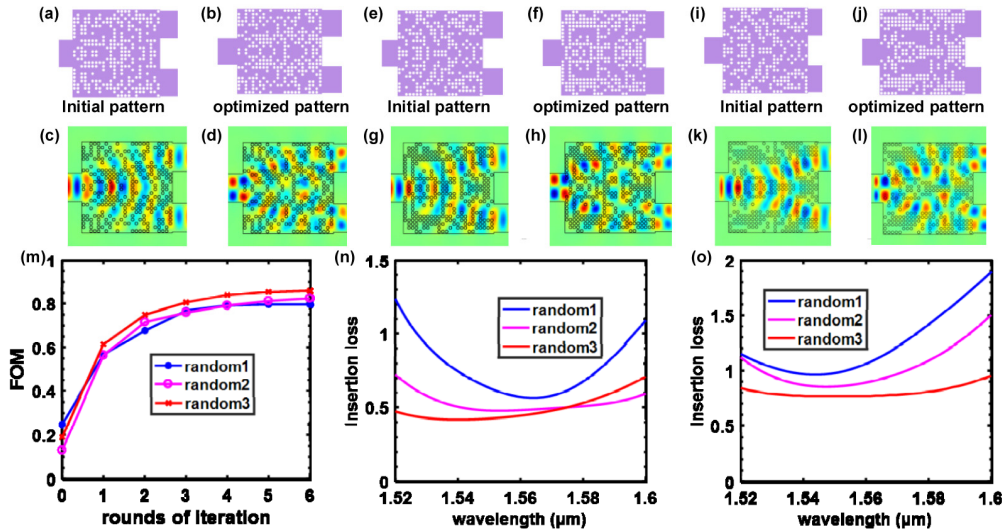


Fig. 4. (a)–(d), (e)–(h) and (i)–(l) The initial and optimized pattern pictures and the corresponding simulated optical field evolutions of H_z for TE₀ and TE₁ for different random initial patterns, respectively. (m) The calculated FOMs after every iteration for different random initial patterns. (n) and (o) The corresponding simulated ELs for TE₀ and TE₁ for different random initial patterns, respectively.

We also simulated the mode evolution in inverse-designed subwavelength dual-mode 3 dB power splitters with different footprints of $2.88 \times 2.16 \mu\text{m}^2$, $2.88 \times 2.88 \mu\text{m}^2$ and $2.88 \times 3.6 \mu\text{m}^2$. The initial patterns are also random. The optimized patterns are shown in Figs. 5(a)-5(b), Figs. 5(e)-5(f) and Figs. 5(i)-5(j), respectively. Besides, the corresponding optical field evolution of H_z for TE₀ and TE₁ are illustrated in Figs. 5(c)-5(d), Figs. 5(g)-5(h) and Figs. 5(k)-5(l), respectively. As expected, the working mechanisms of all the ultracompact power splitter with different footprints also converge to the proposed equivalent model based on subwavelength structure DMC. The calculated FOMs for all the patterns after every iteration are also illustrated in Fig. 5(m). The corresponding transmission spectra for TE₀ and TE₁ of the three optimized devices with different footprints are shown in Figs. 5(n) and 5(o), respectively. The simulation results indicate that the optimized devices exhibits better performance as the length of device increases. However, there is a tradeoff between the calculation time and device footprint. As a result, the footprint of the device is finally chosen as $2.88 \times 2.88 \mu\text{m}^2$, which may be the most compact footprint for a dual-mode 3 dB power splitter to the best of our knowledge.

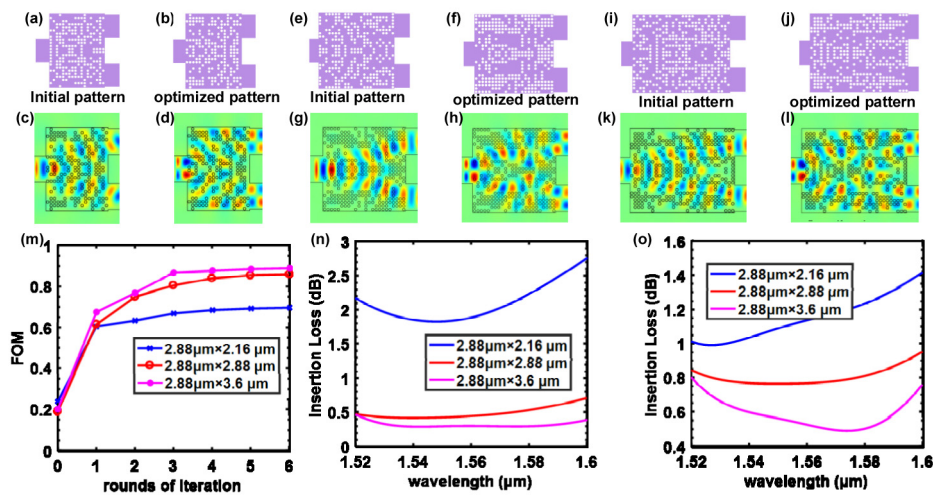


Fig. 5. (a)–(d), (e)–(h) and (i)–(l) The initial and optimized pattern pictures and the corresponding simulated optical field evolutions of Hz for TE₀ and TE₁ for the different footprints of $2.88 \times 2.16 \mu\text{m}^2$, $2.88 \times 2.88 \mu\text{m}^2$ and $2.88 \times 3.6 \mu\text{m}^2$, respectively. (m) The calculated FOMs after every iteration for the different footprints. (n) and (o) The corresponding simulated ELs for TE₀ and TE₁ for the different footprints, respectively.

3. Experiment results

We fabricated and experimentally demonstrated the ultracompact dual-mode 3 dB power splitter based on subwavelength structure DMC. Firstly, the optimized nanopattern was formed on SOI platform with a 220 nm-thick top silicon layer using electron-beam lithography (EBL) system (Vistec EBPG 5000 Plus). Then an inductively coupled plasma (ICP) etcher (Plasma lab System100) was utilized to transfer the mask to the silicon device layer. To generate and characterize the TE₀ or TE₁ signals separately, subwavelength (DE) MUXs were also designed and fabricated [28]. Besides, a reference MDM system was also fabricated on the same chip to evaluate the performance of the dual-mode 3 dB power splitter.

Figure 6(a) shows the top-view scanning electron microscope (SEM) picture of the fabricated test system composed of a dual-mode 3 dB power splitter, a MUX and two DEMUXs. The reference MDM system is shown in Fig. 6(d). Figures. 6(c) and 6(d) illustrate the detailed SEM images of the fabricated dual-mode 3 dB power splitter and DEMUX, respectively. Here, a broad amplified spontaneous emission (ASE) light source and an optical spectrum analyzer (Yokogawa AQ6370C-20) were utilized to measure the transmission spectrum of the fabricated device. From the spectral transmission scans for each combination of input and output ports, the performance of the reference MDM system was characterized and presented in Fig. 6(e), in which, for example, “1-2” denotes the spectral transmission from input port 1 (I1) to output port 2 (O2). TE₀ and TE₁ are excited when the light is launched in input port I3 and I4, respectively. The measured insertion losses and XTs were less than 1.5 dB and lower than -24 dB for both TE₀ and TE₁ from 1.52 μm to 1.6 μm . Similarly, the transmission spectra of the fabricated dual-mode 3 dB power splitter were characterized and obtained, as shown in Figs. 6(f)- 6(h). The measured average ELs and XTs (normalized to the referenced MDM system) for both modes were less than 1.5 dB and -20 dB over a wavelength range from 1520 to 1580 nm, respectively. The ELs for the fabricated devices were measured by three times, as shown in Figs. 6(f) and 6(g). Shaded areas indicate minimum and maximum measured values across the fabricated devices, and solid lines indicate the average values. The measured average standard deviations for the transmission spectrum of ‘1-2’, ‘1-3’, ‘2-1’ and ‘2-4’ are 0.32 dB, 0.16 dB, 0.21 dB and 0.15 dB, respectively. Moreover, the measured average EL imbalances for TE₀ and TE₁ were 0.08 dB

and 0.07 dB, respectively. The measured results indicate that the fabricated nanostructured device has an approximate 50:50 power splitter for both modes from 1520 to 1580 nm. The consistent experimental performance with the simulated results exhibited that the PhC-like nanostructured devices were robust to fabrication errors.

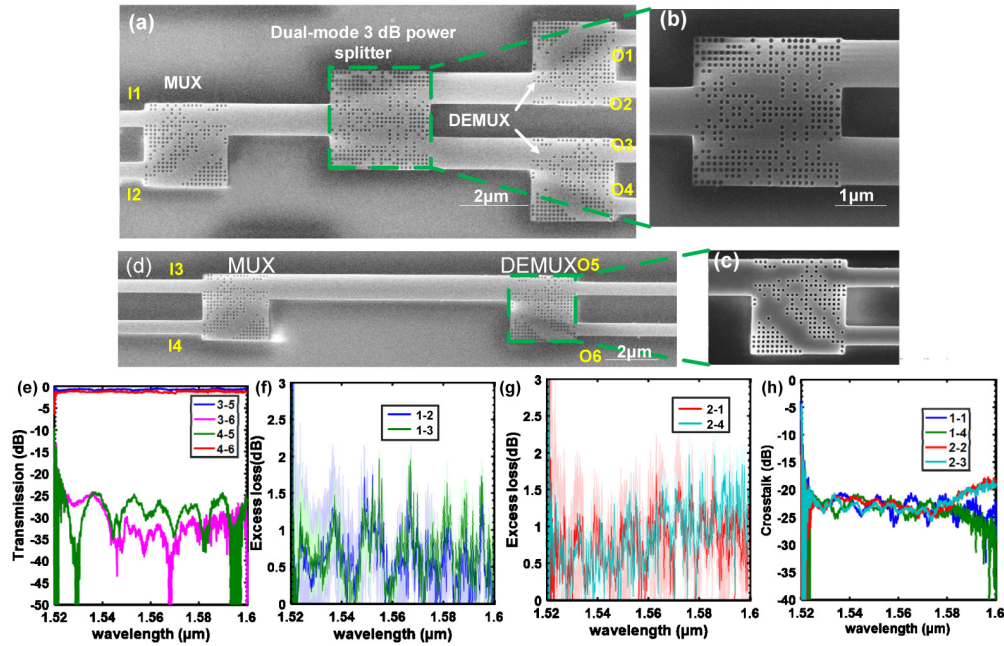


Fig. 6. (a) SEM image for the entire fabricated device composed of a dual-mode 3 dB power splitter and three (DE) MUXs. (b) and (c) The detailed SEM images for dual-mode 3 dB power splitter and DEMUX. (d) SEM picture for the reference MDM system. (e) The normalized measured transmission spectra for the fabricated reference MDM system. (f) and (g) The measured ELs for both modes for the fabricated 3 dB power splitter, respectively. Shaded areas indicate minimum and maximum measured values across the fabricated devices, and solid lines indicate the average values. (h) The measured XTs for both modes for the fabricated 3 dB power splitter.

4. Conclusion

We propose and experimentally demonstrate an ultracompact broadband dual-mode 3 dB power splitter based on subwavelength structure DMC using the inverse design method. Numerical simulations indicate that the inverse-designed nanostructures could enable one to flexibly manipulate modal optical field evolution and implement ultracompact and high performance dual-mode 3 dB power splitter. The axisymmetric topology constraint enables the nanostructures with random-generated initial patterns or different footprints usually converge to our proposed equivalent conventional waveguide model and realize a strict 50:50 splitting ratio for both modes. The fabricated device exhibits high performance with average ELs less than 1.5 dB and XTs lower than -20 dB from 1.52 to 1.58 μm for both modes. Meanwhile, an approximate 50:50 power splitter for both modes from 1.52 to 1.58 μm was achieved, which was consistent with the numerical simulations. The footprint of the fabricated device was only $2.88 \times 2.88 \mu\text{m}^2$, which is two orders of magnitude smaller than that of conventional one. The ultracompact broadband dual-mode 3 dB power splitter will show greatly potential application in densely integrated photonic MDM systems for on-chip optical interconnect.

Funding

National Natural Science Foundation of China (61775069); Fundamental Research Funds for the Central Universities, Huazhong University of Science and Technology (HUST) (2017KFXKJC002).

References

1. D. Dai and J. E. Bowers, "Silicon-based on-chip multiplexing technologies and devices for Peta-bit optical interconnects," *Nanophotonics* **3**(4-5), 283 (2014).
2. J. Wang, S. He, and D. Dai, "On-chip silicon 8-channel hybrid (de)multiplexer enabling simultaneous mode- and polarization-divisionmultiplexing," *Laser Photonics Rev.* **8**(2), 18–22 (2014).
3. J. Wang, P. Chen, S. Chen, Y. Shi, and D. Dai, "Improved 8-channel silicon mode demultiplexer with grating polarizers," *Opt. Express* **22**(11), 12799–12807 (2014).
4. Y. Ding, J. Xu, F. Da Ros, B. Huang, H. Ou, and C. Peucheret, "On-chip two-mode division multiplexing using tapered directional coupler-based mode multiplexer and demultiplexer," *Opt. Express* **21**(8), 10376–10382 (2013).
5. L. W. Luo, N. Ophir, C. P. Chen, L. H. Gabrielli, C. B. Poitras, K. Bergmen, and M. Lipson, "WDM-compatible mode-division multiplexing on a silicon chip," *Nat. Commun.* **5**(1), 3069 (2014).
6. J. B. Driscoll, R. R. Grote, B. Souhan, J. I. Dadap, M. Lu, and R. M. Osgood, "Asymmetric Y junctions in silicon waveguides for on-chip mode-division multiplexing," *Opt. Lett.* **38**(11), 1854–1856 (2013).
7. Y. Zhang, Y. He, Q. Zhu, C. Qiu, and Y. Su, "On-chip silicon photonic 2 × 2 mode- and polarization-selective switch with low inter-modal crosstalk," *Photon. Res.* **5**(5), 521–526 (2017).
8. L. Yang, T. Zhou, H. Jia, S. Yang, J. Ding, X. Fu, and L. Zhang, "General architectures for on-chip optical space and mode switching," *Optica* **5**(2), 180–187 (2018).
9. H. Xu and Y. Shi, "Dual-mode waveguide crossing utilizing taper-assisted multimode-interference couplers," *Opt. Lett.* **41**(22), 5381–5384 (2016).
10. W. Chang, L. Lu, X. Ren, D. Li, Z. Pan, M. Cheng, D. Liu, and M. Zhang, "Ultracompact dual-mode waveguide crossing based on subwavelength multimode-interference couplers," *Photon. Res.* **6**(7), 660–665 (2018).
11. H. Xu and Y. Shi, "Ultra-Sharp Multi-Mode Waveguide Bending Assisted with Metamaterial-Based Mode Converters," *Laser Photonics Rev.* **12**(3), 1700240 (2018).
12. C. Sun, Y. Yu, G. Chen, and X. Zhang, "Ultra-compact bent multimode silicon waveguide with ultralow inter-mode crosstalk," *Opt. Lett.* **42**(15), 3004–3007 (2017).
13. W. Chang, L. Lu, D. Liu, and M. Zhang, "Ultra-compact silicon multi-mode waveguide bend based on subwavelength asymmetric Y-junction," Optical Fiber Communication Conference. Optical Society of America, (2018).
14. Y. Luo, Y. Yu, M. Ye, C. Sun, and X. Zhang, "Integrated dual-mode 3 dB power coupler based on tapered directional coupler," *Sci. Rep.* **6**(1), 23516 (2016).
15. H. Xu and Y. Shi, "Ultra-broadband dual-mode 3 dB power splitter based on a Y-junction assisted with mode converters," *Opt. Lett.* **41**(21), 5047–5050 (2016).
16. L. Han, B. P. P. Kuo, N. Alic, and S. Radic, "Ultra-broadband multimode 3dB optical power splitter using an adiabatic coupler and a Y-branch," *Opt. Express* **26**(11), 14800–14809 (2018).
17. A. Y. Piggott, J. Lu, K. G. Lagoudakis, J. Petykiewicz, T. M. Babinec, and J. Vučković, "Inverse design and demonstration of a compact and broadband on-chip wavelength demultiplexer," *Nat. Photonics* **9**(6), 374–377 (2015).
18. B. Shen, P. Wang, R. Polson, and R. Menon, "An integrated-nanophotonics polarization beamsplitter with footprint," *Nat. Photonics* **9**(6), 378–382 (2015).
19. Z. Yu, H. Cui, and X. Sun, "Genetic-algorithm-optimized wideband on-chip polarization rotator with an ultrasmall footprint," *Opt. Lett.* **42**(16), 3093–3096 (2017).
20. K. Xu, L. Liu, X. Wen, W. Sun, N. Zhang, N. Yi, S. Sun, S. Xiao, and Q. Song, "Integrated photonic power divider with arbitrary power ratios," *Opt. Lett.* **42**(4), 855–858 (2017).
21. M. Teng, K. Kojima, T. Koike-Akino, B. Wang, C. Lin, and K. Parsons, "Broadband SOI mode order converter based on topology optimization," in *Optical Fiber Communication Conference*, OSA Technical Digest (Optical Society of America), paper Th2A.8 (2018).
22. L. Lu, D. Liu, F. Zhou, D. Li, M. Cheng, L. Deng, S. Fu, J. Xia, and M. Zhang, "Inverse-designed single-step-etched colorless 3 dB couplers based on RIE-lag-insensitive PhC-like subwavelength structures," *Opt. Lett.* **41**(21), 5051–5054 (2016).
23. A. Y. Piggott, J. Petykiewicz, L. Su, and J. Vučković, "Fabrication-constrained nanophotonic inverse design," *Sci. Rep.* **7**(1), 1786 (2017).
24. Y. Wang, S. Gao, K. Wang, and E. Skafidas, "Ultra-broadband and low-loss 3 dB optical power splitter based on adiabatic tapered silicon waveguides," *Opt. Lett.* **41**(9), 2053–2056 (2016).
25. Y. Zhang, A. Hosseini, X. Xu, D. Kwong, and R. T. Chen, "Ultralow-loss silicon waveguide crossing using Bloch modes in index-engineered cascaded multimode-interference couplers," *Opt. Lett.* **38**(18), 3608–3611 (2013).

26. T. Uematsu, Y. Ishizaka, Y. Kawaguchi, K. Saitoh, and M. Koshiba, "Design of a Compact Two-Mode Multi/Demultiplexer Consisting of Multimode Interference Waveguides and a Wavelength-Insensitive Phase Shifter for Mode-Division Multiplexing Transmission," *J. Lightwave Technol.* **30**(15), 2421–2426 (2012).
27. Lumerical FDTD solutions, <https://www.lumerical.com>.
28. W. Chang, L. Lu, X. Ren, D. Li, Z. Pan, M. Cheng, D. Liu, and M. Zhang, "Ultra-compact mode (de) multiplexer based on subwavelength asymmetric Y-junction," *Opt. Express* **26**(7), 8162–8170 (2018).